**Article:**

eprints@whiterose.ac.uk
https://eprints.whiterose.ac.uk/

# A validated numerical investigation of the effects of high blockage ratio and train and tunnel length upon underground railway aerodynamics

Daniel Cross[a,*], Ben Hughes[a], Derek Ingham[a], Lin Ma[a]

[a]*Department of Mechanical Engineering, University of Sheffield, Sheffield, UK, S1 3JD*

## Abstract

In order to ensure the safety and comfort of passengers and staff, an underground railway requires an extensive ventilation and cooling system. One mechanism for underground railway ventilation is the movement of air induced by trains, termed the 'piston effect'. This study investigated the effect of altering the blockage ratio of an underground train upon the ventilating air flows driven by a train. First a computational model was developed and validated with experimental data from literature. This model was scaled to represent an operational underground railway with high blockage ratio and the blockage ratio varied to evaluate the effects upon ventilation. The results of this study show that ventilating air flows can be increased significantly during periods of constant train motion and acceleration, by factors of 1.4 and 2 respectively, but that the train drag will increase at the same rate. During deceleration negligible increases in ventilation flows are found but drag increases by a factor of 4.

*Keywords:* Underground railways, Aerodynamics, High blockage ratio, Ventilation, Computational fluid dynamics

## 1. Introduction

Underground railways have been in existence since the opening of the Metropolitan Railway in London, UK in 1863, and new systems continue to be developed and existing ones upgraded or expanded [1, 2]. In order to ensure the safety and comfort of passengers and staff, an underground railway requires an extensive
5  ventilation and cooling system. This is needed firstly to provide for human physiological and comfort requirements but also to manage air conditions in emergency situations, such as fires. Underground railway ventilation is a complex and dynamic system, influenced by many different flows and conditions including those induced by train movement.

Train induced air flows in tunnels, also known as the 'piston effect', are driven by the presence of a tunnel
10  wall adjacent to a moving train. When moving through open space, the air displaced by a train can move to the side of the vehicle in all directions. However, when the train passes through a tunnel, the ability for the air to displace to the sides of the vehicle is reduced. As the air cannot completely pass to the rear of the train, much of the air will flow in front of the train. This creates a high pressure region at the train front whilst at the back of the train a low pressure region is formed, along with the creation of a wake, which acts
15  to suck air from behind the train. The pressure difference between the front and back induces air flow down the side of the train.

Train induced air flows can have a positive impact on the underground railway environment through the ventilation of tunnels and station areas but can also introduce undesirable effects such as high pressures and platform velocities which may cause discomfort to people or damage to the infrastructure. Generally,
20  underground railways are designed with features to enhance and control train induced air flows. Draught relief shafts may be constructed near stations to allow air exchange with the outside environment, the reduction

---

*Corresponding author
Email address:* `dcross1@sheffield.ac.uk` (Daniel Cross)

of high pressures and the reduction of platform air velocities. Air shafts may be utilised in between stations to enhance air exchange operating either mechanically or non-mechanically. Cross passages between running tunnels are often provided to reduce high pressure transients, train drag and high platform velocities. An extensive study was carried out in the 1970s under the direction of the US Department of Transportation into the design of underground railways and has since been used as a major guide for the construction of many systems [3].

In existing high blockage ratio underground railways significant problems are experienced with managing the ventilation, often resulting in issues with overheating. In this paper the effect of altering the blockage ratio in such an environment is investigated to understand the impact on tunnel air flows and train drag, and hence the potential for realising enhanced ventilating air flows.

## 2. Previous Work

In recent years, numerical and experimental work has been performed in order to investigate the effects of train induced flows on underground railway environments. Pope et al. [4] performed an extensive parametric study of an underground railway system to investigate how air velocities and temperatures are affected by train induced flows in various underground configurations. Lin et al. [5] considered the performance of draught relief shafts through experimental measurements and numerical simulations. Eckford and Pope [6] studied the effect of increasing the air exchange through train induced flows, draught relief or forced ventilation. It was found that if the air exchange is increased 1.6 times, by whichever means, then a $4\,^{\circ}$C reduction in tunnel temperatures could be achieved. Ono et al. [7] analysed the scheduling of mechanical ventilation systems based on train movements. They found that, for most of the day, train induced flows were sufficient for ventilation and that only short periods of mechanical assistance were required. Kim and Kim [8] used experimental and numerical methods to investigate the behaviour of train induced flows and train aerodynamics. This work was later extended by Kim and Kim [9] to consider the effect of ventilation shaft locations. Ke et al. [10] studied the effect of ventilation shaft length, cross sectional area and train speed on the ventilation rate and the thermal environment. They found that increasing air flows decrease tunnel temperatures up to a point after which heat from traction and braking undermine any further improvements. El-Bialy and Khalil [11] investigated the thermal comfort on a station in the Cairo Metro using experimental and numerical methods. Yan et al. [12] compared the performance of underground railway tunnels with one or two ventilation shafts. Gonzalez et al. [13] performed a numerical investigation of train induced flows in a tunnel, incorporating mechanical and non-mechanical ventilation shafts, and show that running mechanical shafts in support of train induced air flows can result in energy savings. Xue et al. [14] analysed the effect that the location of draft relief shafts and louvres had upon ventilation through numerical analysis and experimental measurements in an operational railway. Huang et al. [15] used the model presented by Kim and Kim [8] to investigate the use of solid curtains at extreme ends of a tunnel in improving ventilation performance. It was found that such devices could improve ventilation rates significantly but practical problems would make implementation difficult. Ampofo et al. [16] considered various methods of delivering cooling in underground railways, with particular attention to the situation in the UK. They showed that the improvement in ventilation capacity can reduce tunnel temperatures but that implementation could prove problematic.

The mechanism of the piston effect itself has also been investigated widely, mainly in the context of high speed trains. Ricco et al. [17] carried out a experimental and numerical investigation into the pressure waves induced by a train running through a tunnel and noted the importance of train nose shape and the presence of a recirculation zone at the train nose. It was also noted that for a constant blockage ratio, the shape of the train nose was not significant. Baron et al. [18] studied the effect of pressure relief devices on the pressure waves generated by high speed trains. Ko et al. [19] studied induced pressures in tunnels through field measurements and found that the cross sectional area of the tunnel is a major influence on the magnitude of induced pressures. It was also found that pressure peaks were proportional to train speed. The performance of trains in tunnels was investigated by Raghunathan et al. [20]. It was found that the shape of a train nose can effect the performance of a high speed train significantly. Many authors have investigated the effect of

2

tunnel hoods on induced pressures. Howe [21] studied the optimal distribution of orifices in a tunnel hood in order to suppress micro pressure waves on train entry. An experimental and numerical investigation was carried out by Bellenoue et al. [22] into the effect of a tunnel hood on pressure waves and found that the reductions in pressure change are independent of blockage ratio. It was found by Mok and Yoo [23] that a hood could reduce the pressure gradients of the compression waves produced by train entry by 20%. Rabani and Faghih [24] found that the speed and blockage ratio of a train are the main factors which affect the pressure wave and the shape of the train effects the gradient in reaching the maximum pressure.

There are a number of factors which influence the behaviour and volume of air flows induced by trains, including train velocity, tunnel and train properties, the frequency of trains and the blockage ratio – the ratio of the train to tunnel cross sectional areas [25, 26].

In most previous work, the blockage ratio is investigated in terms of the influence upon pressure waves, a phenomenon one would wish to reduce. In this work, focus is given to the impact of the blockage ratio on the magnitude of the induced air flows which are useful for ventilation in a low speed, underground railway environment. First a numerical model is developed and validated with available experimental data, and scaled to represent a full scale environment. The effect of the blockage ratio upon train drag and outlet air velocities is investigated with particular consideration given to the different effects of pressure and viscous drag forces. The relationship between tunnel and train length and train drag and outlet air velocities is also presented and interpreted.

## 3. Methodology

A transient, three-dimensional computational fluid dynamics (CFD) simulation was used to model the induced air flows generated by train movement in a tunnel. The study is formed in two parts; a validation and verification of a CFD model of an underground railway and the examination of the effect of high blockage ratio and train and tunnel length upon tunnel air flow.

An idealised scale model representation of an underground railway environment was employed in order to simplify the physical phenomena and modelling process and is modelled using CFD. This model is validated with available experimental results from the literature. The model was scaled geometrically to represent the full scale, the train velocity varied to examine the effects and the geometry altered to represent an existing underground railway operating at high blockage ratio (Victoria Line, London Underground, UK). This process is carried out to establish the impact of blockage ratio and train and tunnel length in current underground railways. The blockage ratio and train and tunnel length are all varied independently and the impact upon tunnel air flows and train drag is shown.

### 3.1. Model Set-up

The scale model configuration used in this study is duplicated from the experimental set-up presented by Kim and Kim [8] and used subsequently by various authors [9, 27, 28]. The model is shown schematically in Figure 1, and describes a 1/20 scale model of an underground railway.
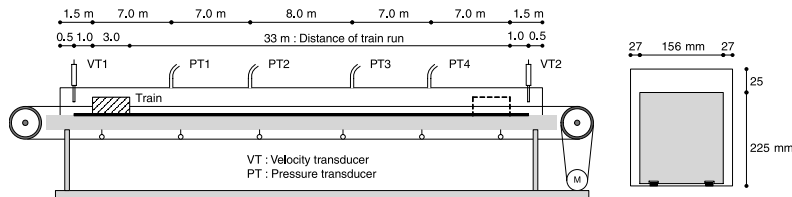


Figure 1: A schematic diagram of the Kim and Kim [8] train and tunnel scale model experimental set-up.

The tunnel does not include any features such as shafts or passages to allow the investigation of the train induced flows without interference from other factors. The set-up consisted of a tunnel, both ends open to the atmosphere, in which a model train was passed. The tunnel was 39 m long, 0.21 m wide and 0.25 m high,

3

while the train was $3\,\text{m}$ long, $0.156\,\text{m}$ wide and $0.225\,\text{m}$ high. The tunnel height is given as $0.25\,\text{m}$, the train height as $0.225\,\text{m}$ and the vertical upper gap between the train and tunnel as $0.025\,\text{m}$, but the lower vertical gap between the train and tunnel is not stipulated. In this work a value of $0.003\,\text{m}$ is used to represent a gap under the train without reducing the height of the train significantly.

The train starting position is with the rear $1.5\,\text{m}$ from the tunnel entrance portal, it was accelerated at $1\,\text{ms}^{-2}$ for $3\,\text{s}$, ran at a constant speed of $3\,\text{ms}^{-1}$ for $8\,\text{s}$ and then decelerated at $-1\,\text{ms}^{-2}$ for $3\,\text{s}$, to an end position with the front $1.5\,\text{m}$ from the tunnel exit portal. The train remained within the confines of the tunnel for the entire period of travel. Here we refer to the tunnel entrance as the portal which the train is travelling away from and the tunnel exit as the portal the train is travelling towards. Kim and Kim [8] used transducers to take pressure and velocity readings at four and two points, respectively, in the positions shown in Figure 1. The pressure readings were at the tunnel roof and the velocity readings were in the centre of the tunnel cross section. No details were given regarding the measurement equipment used nor of any uncertainties.

### 3.1.1. Computational Domain

The numerical domains investigated were produced in ICEM [29] using a hexahedral grid structure. The grid was formed so that smaller cells were concentrated around the front, rear and walls of the train and the walls of the tunnel to provide sufficient resolution in these regions and larger cells far from the train in order to improve computational efficiency. The final grid structure around the train front is shown in Figure 2. A grid convergence test was carried out and a grid with sufficient accuracy was found that contains 1388838 cells. A time step size convergence study was also conducted giving a time step size of $0.01\,\text{s}$ as acceptable.

The numerical modelling was performed using the Ansys Fluent [30] commercial CFD software package. In order to simulate the train movement, the dynamic meshing option in Ansys Fluent, specifically the dynamic layering method, was utilised as outlined by Huang et al. [27]. This was applied by first dividing the computational domain into three fluid zones; a near field around the train and two far fields ahead of and behind this zone. The near field zone is moved forward at the specified train speed and layers of cells added to the zone behind and removed from the zone ahead of the train. In this way the dynamic meshing process is simplified and the fluid zone around the train can remain unaltered. The use of a hexahedral grid, shown in Figure 2, allowed the use of dynamic layering.
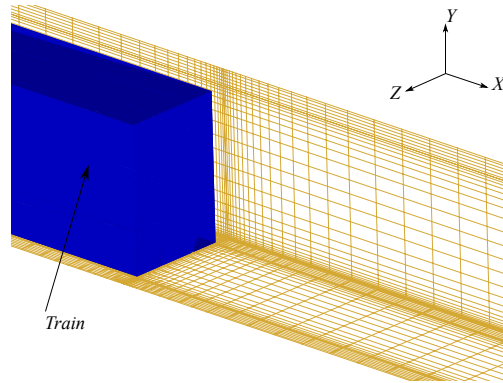


Figure 2: Hexahedral grid around the train front.

In this study, the unsteady air flows are treated as an incompressible fluid [3]. This is justified as velocities of trains in an underground railway are relatively low (average of $9\,\text{ms}^{-1}$ and maximum of $27\,\text{ms}^{-1}$ in London Underground for example) and thus compressible effects are moderate, given that the flow Mach number is small and there is an absence of tunnel features which may create compressible effects. For the unsteady, incompressible fluid flow in an underground railway, the Reynolds-averaged Navier Stokes equations are solved using Fluent.

The $k-\epsilon$ RNG model is utilised in this work due to it's suitability on the investigation of train induced air

flows, in which it was found to perform well [14, 15]. Near wall flows were modelled using the standard wall function, a wall function approach. This was to reduce the computational time of the transient calculations in comparison with a near wall modelling approach. The first cell heights on the walls of the model are chosen so that the non-dimensional $y^+$ value is maintained in the recommended range of $30 < y^+ < 300$, where $y^+ = \frac{\rho u_\tau y}{\mu}$ and $u_\tau$, $y$, $\rho$ and $\mu$ are the friction velocity, distance from the wall, fluid density and dynamic viscosity respectively [30].

The governing equations are solved by use of the finite volume method on an unstructured grid. In this work the PISO pressure-velocity coupling method is adopted to solve the governing equations. The QUICK interpolation scheme is used for the discretisation of the convection terms and the PRESTO scheme to treat the pressure interpolation, for improved performance in conditions with adverse pressure gradients. Convergence criteria for the continuity, momentum, $k$ and $\epsilon$ residual equations were set as $1 \times 10^{-5}$ and additionally the pressure and velocity were monitored at various points within the domain. Mass conservation within the computational domain was also monitored to ensure conservation at every time step.

### 3.1.2. Boundary Conditions

At the tunnel inlet and outlet, an outlet boundary condition with a static pressure of $0\,\mathrm{Pa}$ was applied. This value is given relative to an operating pressure, set at atmospheric pressure. The boundary conditions allow for the dynamic pressure (sometimes called the velocity pressure) to vary while the static pressure is fixed. This allows pressure changes at the boundaries, such as when the train approaches the outlet. An investigation was undertaken of different boundary condition combinations, including pressure inlet and outlet and periodic conditions, however this combination was found to provide good accuracy when compared to Kim and Kim [8] and the approach is in agreement with that of Khayrullina et al. [31].

### 3.2. Model Scaling

The model outlined in Section 3.1 is a $^1/_{20}$ scale model of an idealised underground railway. In order to be confident that the scale model provides useful results that represent the flow behaviour that would exist in a full scale environment then the model was scaled and similarity shown [32]. This model was scaled in terms of $Re_{max}$ so the conditions at more realistic velocities could be investigated. The scaling process presented in this work is derived from the Subway Environmental Design Handbook [3].

### 3.2.1. Similarity

Similarity in ensured through the observation of three criteria: geometric, kinematic and dynamic similarity. The scale model was scaled geometrically by a constant factor of 20 in all dimensions for a full scale model. The scale and full scale models are referred to as $M_1$ and $M_2$ respectively.

Dynamic and kinematic similarity are ensured through maintaining the Reynolds number and drag coefficient between the scale and scaled models. The use of these coefficients is deduced through use of the Buckingham $\pi$ theorem which shows that these two coefficients account for the properties of interest [33].

The Reynolds number is given as

$$Re = \frac{\rho u_{tr} H_t}{\mu}. \tag{1}$$

In Equation (1), $u_{tr}$ is the train velocity, $H_t$ is the tunnel height, the density $\rho = 1.225\,\mathrm{kg m^{-3}}$ and the dynamic viscosity $\mu = 1.7894 \times 10^{-5}\,\mathrm{kg s^{-1} m^{-1}}$ (at $288.15\,\mathrm{K}$ air temperature). The kinematic properties of the two models $M_1$ and $M_2$ are shown in Table 1, where $^{du_{tr}}/_{dt}$ is the rate of acceleration and deceleration and $t_T$ is the total travel time.

Table 1: Kinematic parameters for models $M_1$ and $M_2$.

| Model | $u_{tr}^{max}\,(\mathrm{ms^{-1}})$ | $^{du_{tr}}/_{dt}\,(\mathrm{ms^{-2}})$ | $t_T\,(\mathrm{s})$ |
|---|---|---|---|
| $M_1$ | 3.00 | $\pm 1.00$ | 14.0 |
| $M_2$ | 0.15 | $\pm 1.25 \times 10^{-4}$ | 5600.0 |

5

The travel times for model $M_2$ are altered in order to account for the scaling. The rate of acceleration and deceleration is altered for case $M_2$ in order for the phases of acceleration and deceleration to take up the same proportion of the total time of train movement as for case $M_1$. The Reynolds number at maximum train velocity $Re_{max}$ for both $M_1$ and $M_2$ was $5.134 \times 10^4$. Since the geometries are geometrically similar, and the $Re_{max}$ is consistent in both cases, kinematic similarity has been ensured.

*3.3. $Re_{max}$ variation*

The velocity of the scaled model $M_2$ does not represent what would be considered a realistic velocity for an underground railway. To assess the effect of an increased, and more realistic, train velocity the maximum velocity of the train in model $M_2$ is increased as shown in Table 2, along with the rate of acceleration and deceleration.

Table 2: $Re_{max}$ scaling parameters for the model $M_2$.

| Case $(Re_{max})$ | $u_{tr}^{max}$ (ms$^{-1}$) | $du_{tr}/dt$ (ms$^{-2}$) | $t_T$ (s) |
|---|---|---|---|
| $5.134 \times 10^4$ | 0.15 | $\pm 1.250 \times 10^{-4}$ | 5600.000 |
| $8.215 \times 10^5$ | 2.40 | $\pm 0.032$ | 350.000 |
| $1.314 \times 10^7$ | 38.40 | $\pm 8.192$ | 21.875 |

The cases are identified by the Reynolds number at maximum train velocity, $Re_{max}$. This is used as a convenient description of each case in Table 2, while each case will have a different average and a constantly varying instantaneous value of Reynolds number. The rate of acceleration and deceleration is again altered so that the time taken for acceleration and deceleration is the same proportion of the total travel time.

The scaled geometry, with train and tunnel lengths of 120 m and 1170 m respectively, is used as a reference case ($M_2(120, 1170)$) and subsequently the $Y$ and $Z$ dimensions, as shown in Figure 2, were scaled by a factor of 0.6238. This is to arrive at a model ($M_3$) with certain parameters similar to a current underground railway operating at a high blockage ratio (Victoria Line, London Underground, UK) [34, 35].

Further $Re_{max}$ variation was performed on model $M_3$, with the parameters shown in Table 3. The Reynolds number scaling was performed here for a second time to investigate the effects of the $M_2$ to $M_3$ scaling.

Table 3: Reynolds number scaling parameters for model $M_3$.

| Case $(Re_{max})$ | $u_{tr}^{max}$ (ms$^{-1}$) | $du_{tr}/dt$ (ms$^{-2}$) | $t_T$ (s) |
|---|---|---|---|
| $5.1245 \times 10^5$ | 2.4000 | $\pm 0.032000$ | 487.500 |
| $8.2150 \times 10^5$ | 3.8474 | $\pm 0.082236$ | 304.317 |
| $4.1000 \times 10^6$ | 19.2000 | $\pm 2.048000$ | 60.938 |
| $8.1992 \times 10^6$ | 38.4000 | $\pm 8.192000$ | 30.469 |
| $4.1000 \times 10^6$ | 19.2000 | $\pm 1.000000$ | 70.763 |

The acceleration/deceleration rate for the $Re_{max} = 4.100 \times 10^6$ case in Table 3 is altered to represent a more realistic value of $\pm 1$ ms$^{-1}$, as the higher rate is not representative of an actual railway. In this case the rate of acceleration and deceleration results in the train spending a longer period of time in these phases of travel, as a proportion of total travel time.

## 4. Validation

*4.1. $^1/_{20}$ Scale Model*

Results for the scale model case $M_1$ correspond to the positions of the four pressure and two velocity transducers used in the Kim and Kim [8] experimental study. Results are given in terms of a pressure coefficient,

$$C_p = \frac{p}{\frac{1}{2}\rho u_*^2} \tag{2}$$

6

and velocity coefficient $u/u_*$, where $u_*$ is a reference velocity, in this case the maximum train velocity $u_{tr}^{max}$. The maximum train velocity is used as a fixed reference as the use of an instantaneous velocity would mean that the coefficient would vary due to two variables hence making interpretations difficult. This approach was used by Rabani and Faghih [24]. Comparison of the experimental and numerical results is shown in Figure 3. The vertical lines in Figure 3, and throughout this paper, indicate the three phases of train motion: acceleration, constant velocity and deceleration.



(a) PT1–PT4                                              (b) VT1 and VT2.
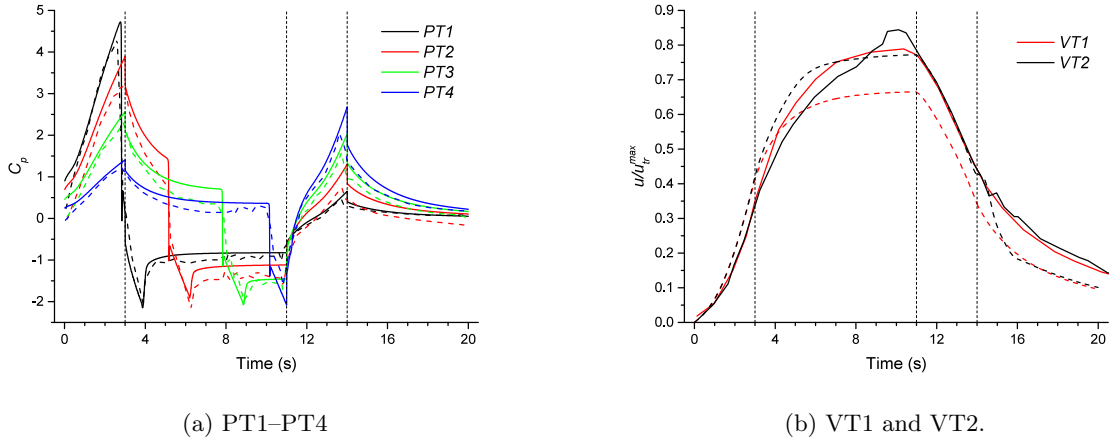
Figure 3: Pressure and velocity coefficients at the positions shown in Figure 1 (— Numerical result, - - Experimental result).

Generally, the numerical results at points corresponding to the pressure transducers in the Kim and Kim [8] work, Figure 3(a), compare well with the available experimental data. Physically it can be seen that during the acceleration and deceleration phases, the pressure rises and during the phases of constant travel the pressure drops and stabilises. This pattern is interrupted for a period at each point during which the train passes, and the effect of which is to cause a sudden drop in pressure followed by a recovery. The pressure coefficients shown here have been well resolved and this shows some improvement from previous work. The cause of this could be due to an improved grid resolution around the front and back of the train.

The results at points corresponding to the locations of the velocity transducers, Figure 3(b), represent the trend of the experimental data well, but with some clear differences. The result at VT1 is generally predicted well during the acceleration phase, but after the inertia of the air is overcome then the velocity is under predicted during the phase of constant travel. This has a corresponding effect upon the accuracy during the deceleration phase. The velocity at VT2 is generally well predicted, particularly in the acceleration and deceleration phases. These phases are dominated by inertial effects, while the constant velocity phase is dominated by viscous effects.

The total displaced air is presented in this work is used to illustrate the ventilating effects of the train movement. This is validated by comparing the time integrals of the measured and numerical velocity curves at VT1 and VT2, which gives differences of 10.0% and 4.7% respectively. These are within acceptable bounds.

The drag coefficient is also a quantity of interest in this work, but is not validated with measured values. The use of the drag coefficient is justified by the validation of the velocity and the relationship between the velocity and drag. Any air velocities generated will be due to the surface of the train acting upon the air, resulting in a force acting upon the train, which is the drag force. So changes in air velocities correspond with changes in drag. Although there are disparities between the measured and numerical values at VT1 and VT2, the acceptable agreement over the time integrals, and for the purposes of the relative comparison of drag in the parametric study shown within this paper the validation is considered sufficient.

7

## 5. Model Scaling from $M_1$ to $M_2$

To ensure that the scale model represents the full scale environment, geometric and kinematic scalings are carried out and dynamic similarity ensured. The results of the scaling are presented in terms of the train drag coefficient and velocity coefficient at the tunnel outlet as a function of the non-dimensional time $T = t/t_T$, where $t_T$ is the total time of train movement. The drag coefficient is defined as

$$C_D = \frac{F_D}{\frac{1}{2}\rho A_{tr} u_*^2} \tag{3}$$

where $F_D$ is the total drag force upon the train acting in the direction opposite to train travel and $A_{tr}$ is the frontal area of the train.

The maximum train velocity is again used as a fixed reference as the use of an instantaneous velocity would mean that the coefficient would vary due to two variables, hence making interpretations difficult. In this paper the drag coefficient takes both positive and negative values to illustrate that the drag may be acting in the direction of train travel or the converse.

The drag and velocity coefficients for the case $Re_{max} = 5.134 \times 10^4$ for models $M_1$ and $M_2$ are shown in Figure 4, along with a range of $Re_{max}$ for model $M_2$.



(a) Train drag coefficient, $C_D$.

(b) Tunnel outlet velocity coefficient, $u/u_{tr}^{max}$.
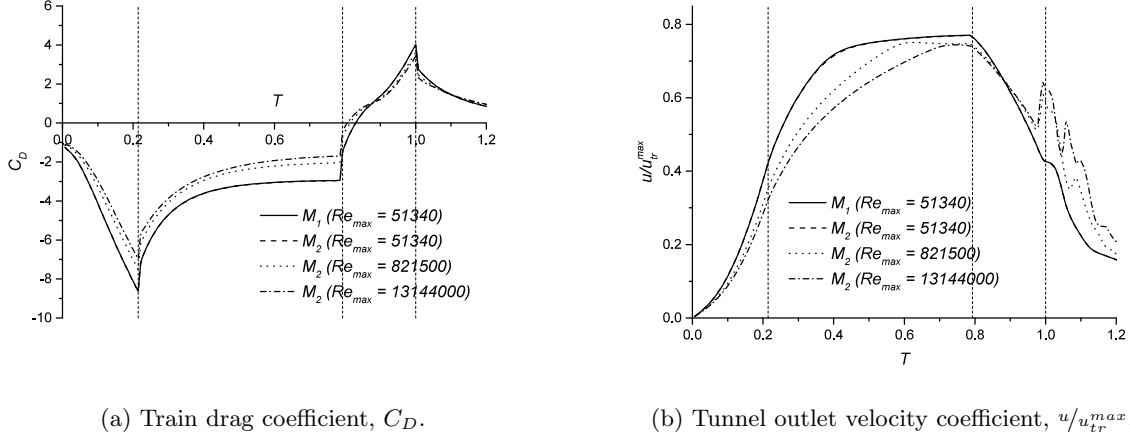
Figure 4: Train drag and tunnel outlet velocities for the models $M_1$ and $M_2$.

The results for $M_1$ and $M_2$ are almost identical, with only minor discrepancies. Combined with the constant Reynolds numbers between the two cases indicates that the scaled up numerical model is acceptable in terms of similarity with the scaled version.

### 5.1. Train Drag

Drag coefficients from the variation of $Re_{max}$ are given in Figure 4(a) during and after train movement. The pattern of behaviour is the same for all cases. During acceleration, the train experiences a significant negative drag. Once the train has reached its maximum velocity then the negative drag slowly reduces asymptotically towards what appears to be a stable value, and this is due to the inertia of the air in the tunnel having being overcome. Finally, almost instantly after the point of deceleration, the drag experienced by the train becomes positive as the body of air behind the train exerts a positive force upon the train. The train continues to experience a positive drag after the train has stopped after $T = 1.0$ and this is due to the continuing movement of air.

The drag coefficient shown in Figure 4(a) decreases as $Re_{max}$ increases due to the changing nature of the forces, both pressure and friction, experienced by the train. As $Re_{max}$ increases, the contribution from

8

pressure drag increases while that from skin friction decreases. At the same time the wake at the rear of the train increases in length and is dominated by pressure forces. Additionally, the flow of air through the annular region increases with increasing $Re_{max}$, thus reducing the contribution from the pressure drag at the front of the train. The initial drag coefficient readings shown in Figure 4(a) are not close to zero due to the train impulsively starting in an entirely quiescent flow field. This effect is also observed in the pressure coefficient shown in Figure 3(a), the impact of which diminished over time.

### 5.2. Tunnel Outlet Velocities

With increasing $Re_{max}$, the velocity coefficient shown in Figure 4(b) indicates a slower rate of increase during the velocity rise induced by the acceleration. This is due to an increased pressure difference across the train, measured between the front and back, and therefore an increased air flow through the annular region from the train nose to tail. At $T = 0.75$, the maximum velocity at the outlet of the tunnel is reached and the coefficient is similar for all the cases investigated. During the deceleration, the coefficient initially indicates little variation between the Reynolds numbers until the flow though the annular region changes direction, due to the air behind the train having a higher velocity than the train such that it is moving from the back to the front and the outlet velocity is greater for higher $Re_{max}$. Once the train has stopped there is an increasingly oscillatory behaviour at the outlet at higher $Re_{max}$ due to the a larger volume of air passing through the annular region towards the train front.

The air flow is driven by the pressure difference across the train. As the pressure difference is high during acceleration an air flow of almost twice the maximum train velocity is observed in the annulus by the end of acceleration for all cases. During the constant velocity phase, initially the pressure difference is greater for higher $Re_{max}$, so a higher annular air flow is observed and therefore a lower outlet velocity. The pressure difference decreases during the constant velocity phase and the annular velocity asymptotes towards a value just greater than the maximum train velocity for all $Re_{max}$ cases. A similar trend to that observed during acceleration is seen during deceleration. As the train slows, the air behind the train creates a higher pressure zone at the train back and this induces a flow through the annular region until the annular flow moves in a positive direction. The change in annular flow from negative to positive results in the drag experienced by the train changing from negative to positive.

### 5.3. Displaced Air Volumes

The total volume of air displaced ($V$) from the tunnel outlet during train motion is shown in Table 4. The total volume of displaced air is also expressed as a fraction of the tunnel volume, $V/V_t$. The displaced air volume is shown to highlight the magnitude of the train air flow in terms of the impact upon ventilation. The total displaced air volume is calculated by integrating the air velocity at the outlet to find the air flow displaced in that time step and then integrated in time to find the total across the whole time period, $t_T$.

Table 4: Total displaced air for model $M_2$.

| Case ($Re_{max}$) | $V$ (m$^3$) | $V/V_t$ () |
|---|---|---|
| $5.134 \times 10^4$ | 8308.18 | 0.507 |
| $8.215 \times 10^5$ | 8156.49 | 0.498 |
| $1.314 \times 10^7$ | 8059.35 | 0.492 |

With increasing $Re_{max}$ the volume of air displaced from the tunnel decreases but only moderately. This is due to the slower rate at which the air in the tunnel reaches the maximum velocity. In all cases, about half of the tunnel volume is displaced through the outlet.

The results from the scale and scaled models show that the behaviour of the quantities presented do not exhibit markedly different characteristics across the range $Re_{max}$ tested. While there are differences in the magnitudes observed, the trends show similar behaviour between the scale model $M_1$ and the full scale model $M_2$ with a realistic velocity.

9

## 6. Model Scaling from $M_2$ to $M_3$

The drag and velocity coefficients for case the $Re_{max} = 5.134 \times 10^4$ for model $M_2(120, 1170)$ and $M_3$ are shown in Figure 5, along with a range of $Re_{max}$ for model $M_3$.



(a) Train drag coefficient, $C_D$.



(b) Tunnel outlet velocity coefficient, $u/u_{tr}^{max}$.
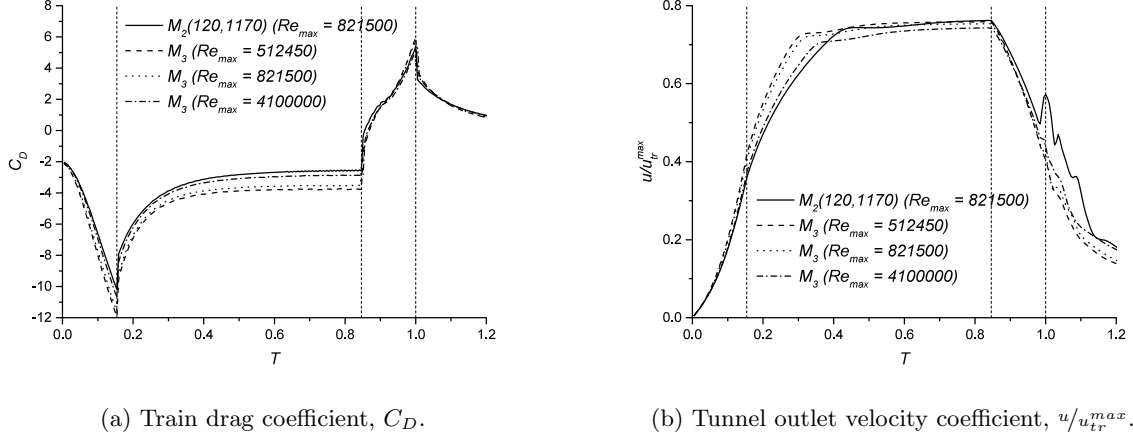
Figure 5: Train drag and tunnel outlet velocities for models $M_2$ and $M_3$

### 6.1. Train drag

As the blockage ratio, the ratio of the train and tunnel perimeters and the Reynolds number are constant between the two models, the differences observed in the train drag must be due to the constant factor scaling of the size of the train and tunnel. For models $M_2$ and $M_3$ for $Re_{max} = 8.215 \times 10^5$, the general behaviour of the train drag is the same for both cases. During the acceleration and constant velocity phases of travel, the drag is consistently higher for model $M_3$ while during the deceleration phase there are only minor differences. With increasing $Re_{max}$, the drag shows the same changes as see with the $M_1$ to $M_2$ scaling. Increased drag is found for the $M_3$ model as compared with $M_2$ as the gap between the train and tunnel wall is smaller in the former case. This restricts the flow of air to the back of the train.

### 6.2. Tunnel Outlet Velocities

The behaviour of the tunnel outlet velocity coefficient follows a similar trend for each case. The smaller annular gap means that the tunnel outlet velocity reaches the maximum value rapidly for each $Re_{max}$ case and this is in contrast to that observed in the model $M_2$. While the rise does become moderately less rapid, the outlet velocity is at it's maximum for most of the constant velocity phase. The behaviour in the $M_2$ model is a much slower rise to the maximum outlet velocity. There is no oscillatory behaviour observed after the train motion, which is present at high $Re_{max}$ for model $M_2$. This is due to the smaller annular gap restricting the flow of air from the back of the train to the front.

### 6.3. Displaced Air Volumes

The total volume of air displaced from the tunnel outlet during the train motion is shown in Table 5. The total volume of displaced air is also expressed as a fraction of the tunnel volume, $V/V_t$.

The displaced air volumes are largely the same for models $M_2$ and $M_3$, at about 0.5 of the tunnel volume, although there is a moderate decrease at the higher $Re_{max}$ cases. This shows that the ventilating air flows are not significantly affected by the velocity of the train nor upon the size of train and tunnel as the value for $M_2$ is 0.510.

Table 5: Total displaced air for model $M_3$.

| Case $(Re_{max})$ | $V$ (m$^3$) | $V/V_t$ () |
|---|---|---|
| $5.1245 \times 10^5$ | 4977.06 | 0.521 |
| $8.2150 \times 10^5$ | 4956.74 | 0.518 |
| $4.1000 \times 10^6$ | 4901.25 | 0.513 |

### 6.3.1. $du/dt$ variation

The impact of variations in $du_{tr}/dt$ are presented in Figure 6 in terms of train drag and outlet velocity coefficients. The solid and dashed vertical lines in Figure 6 indicate the start of acceleration and deceleration phases for cases $du_{tr}/dt = \pm 2.048$ and $du_{tr}/dt = \pm 1$ respectively. The proportion of time which the train is accelerating and decelerating increases for the $du_{tr}/dt = \pm 1$ case. This is due to the acceleration and deceleration phases taking more than double the time in the $du_{tr}/dt = \pm 1$ case than in the $du_{tr}/dt = \pm 2.048$ case and that the time taken for the constant velocity phase reduces in the $du_{tr}/dt = \pm 1$ case.



(a) Train drag coefficient, $C_D$.  (b) Outlet velocity coefficient, $u/u_{tr}^{max}$.
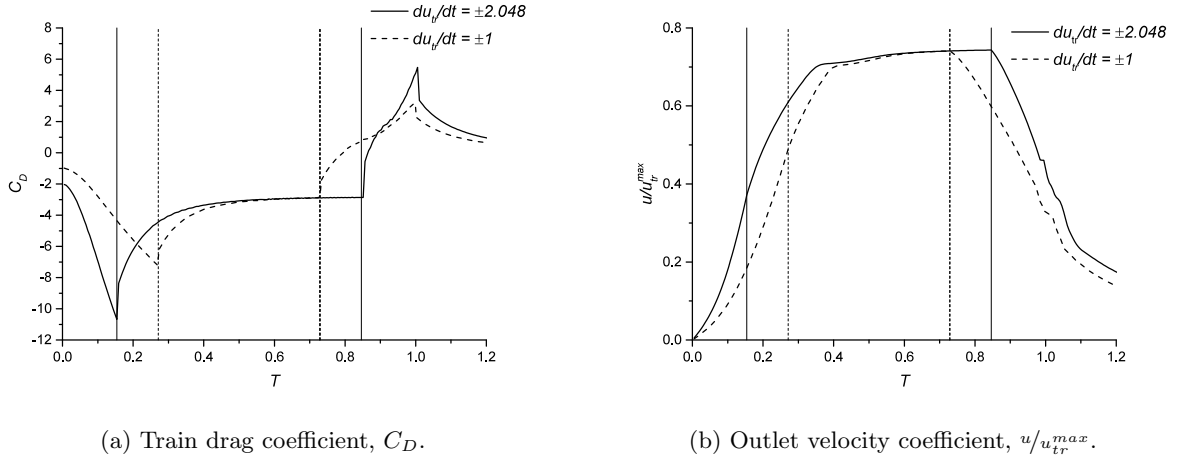
Figure 6: Results for $du_{tr}/dt$ variations for model $M_3$ with $Re_{max} = 4.100 \times 10^7$.

Figure 6(a) shows the drag coefficient during the train motion. For $du_{tr}/dt = \pm 2.048$, the increase in the magnitude of the drag coefficient during acceleration is more rapid and reaches a maximum value 48% of that in the $du_{tr}/dt = \pm 1$ case. Both cases reach a similar value during the constant velocity phase. During deceleration, the $du_{tr}/dt = \pm 2.048$ case again sees a more rapid increase in drag and reaches a higher value than the $du_{tr}/dt = \pm 1$ case, however the differences between the two cases in this phase are less significant. The faster rate of acceleration and deceleration for the $du_{tr}/dt = \pm 2.048$ case means that the overall tunnel velocities are higher, but not during the constant velocity phase. A higher rate of $du_{tr}/dt$ results in an increased tunnel air velocity for only a short period of time as shown in Figure 6(b). This effect only persists for a short time.

The volumes of air displaced from the tunnel outlet as a proportion of the tunnel volume are 0.513 and 0.527 for the $du_{tr}/dt = \pm 2.048$ and $du_{tr}/dt = \pm 1$ cases respectively. Although the $du_{tr}/dt = \pm 1$ outlet velocity does not reach a maximum value as fast as the $du_{tr}/dt = \pm 2.048$ case there is a higher overall volume displacement. However, this is due to the outlet velocity measurements being taken at a single point in the tunnel cross section. Overall the change is acceleration does not significantly effect the total displaced air volume.

## 7. Results and Discussion

The effect of variations in blockage ratio were investigated using model $M_3$ and train and tunnel length using model $M_2$.

### 7.1. Blockage Ratio Variation

The blockage ratio $\beta$ was varied to investigate the effect on train drag, tunnel air flows and the implications for tunnel ventilation. The model $M_3$ is used in this analysis since the dimensions correspond to an existing underground railway operating at high blockage ratio. The blockage ratio is defined as

$$\beta = \frac{A_{tr}}{A_t} \tag{4}$$

where $A_{tr}$ and $A_t$ are the cross sectional areas of the train and tunnel. The $Re_{max} = 4.100 \times 10^6$ case for model $M_3$ with a $1\,\mathrm{ms}^{-2}$ acceleration/deceleration rate is used as a base case, denoted by $\beta_{0.65}$. The blockage ratio is varied following the parameters given in Table 6 and illustrated in Figure 7, where $Y_a$ and $Z_a$ are the $Y$ and $Z$ dimensions of the annular region between the train and tunnel walls, $Y_{tr}$ and $Z_{tr}$ are the $Y$ and $Z$ dimensions of the train and $Y_t$ and $Z_t$ are the $Y$ and $Z$ dimensions of the tunnel.
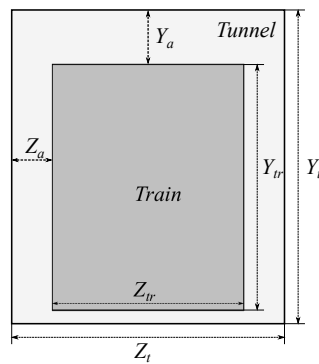


Figure 7: Diagram of blockage ratio variation parameters (cross sectional view).

Table 6: Blockage ratio variation parameters.

| Model | $Y_a$ (m) | $Z_a$ (m) | $\beta$ |
|---|---|---|---|
| $\beta_{0.65}$ | 0.3119 | 0.3369 | 0.65 |
| $\beta_{0.75}$ | 0.2183 | 0.2358 | 0.75 |
| $\beta_{0.78}$ | 0.1871 | 0.2021 | 0.78 |
| $\beta_{0.85}$ | 0.1248 | 0.1347 | 0.85 |

As a train moves through a tunnel in an actual underground railway there are lateral movements in the $Z$ direction generated by the train motion. These changes in the lateral position of the train are not considered here and the train is positioned symmetrically in the $Z$ direction. The lateral movements induced by the train motion do not effect the blockage ratio of the train, hence the prediction of the volume of air displaced will not be adversely affected.

### 7.1.1. Effect on Drag and Velocity

The train drag and tunnel outlet velocity coefficients during and after the train motion are shown in Figure 8.



(a) Train drag coefficient, $C_D$.

(b) Tunnel outlet velocity coefficient, $u/u_{tr}^{max}$.
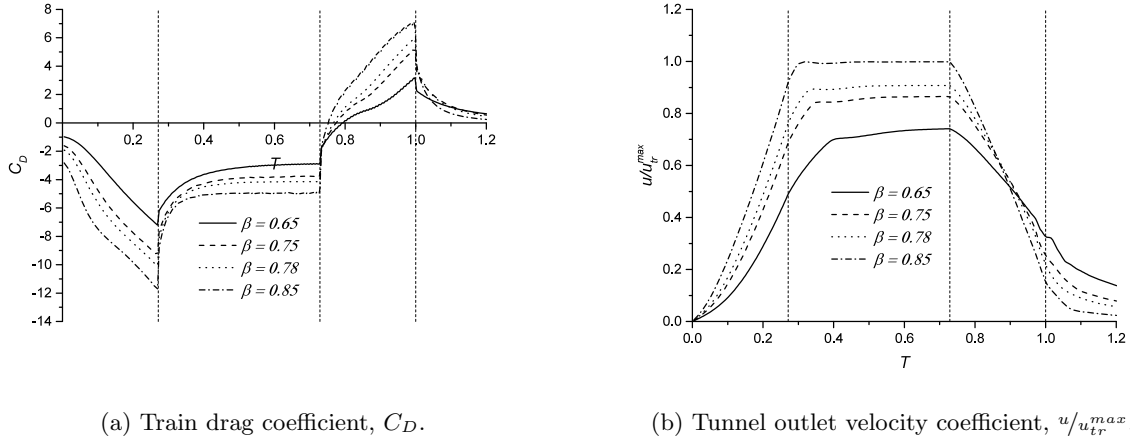
Figure 8: Train drag and tunnel outlet velocities for various blockage ratios.

The result for each blockage ratio exhibits the same behaviour but with increased magnitude for higher blockages. Increasing blockage ratio from 0.65 to 0.85, a 30% increase, increases the drag experienced by the train through the whole period of travel. During acceleration this means an increase in the average drag of 100%. During constant velocity phases there is an increase of 49% in the average drag. During deceleration the train experiences an increased period of positive drag which would have to be opposed by the train brakes. The drag increases by a factor of 4 during deceleration.

Tunnel outlet velocities also indicate a similar behaviour regardless of blockage ratio, but with increased magnitude. During acceleration, higher blockage ratios mean that the maximum outlet velocity is reached more rapidly and the maximum attained velocity is higher. In the case of $\beta = 0.85$, this is close to the maximum train velocity. During the constant velocity phase an increase of 36% in the outlet velocity is observed. During deceleration, the outlet velocities decrease more rapidly at higher blockage ratios due to the train blocking the induced air flows from moving past the train to the outlet. Towards the end of the deceleration, the lower blockage ratio cases give higher velocities than the higher cases. This trend continues after the train has stopped. It is this behaviour which creates the higher positive drag coefficients during deceleration.

### 7.1.2. Pressure Difference

The factors which effect the drag and tunnel air flows are the pressure difference between the train front and back and the air flow in the annular region. The pressure difference between the front and back of the train is shown in Figure 9.

During acceleration the pressure difference increases, which encourages air flow through the annular region. As the blockage ratio increases, the pressure difference increases but the air flow in the annular region decreases due to the contraction in the cross sectional area. The value of the pressure difference and annular region velocity asymptotes to a stable value during the constant velocity phase and display less significant differences.

The changes in pressure throughout the train motion do not indicate that unsafe pressure changes are created at any blockage ratio. The safe level of pressure change is given by the International Union of Railways [37] as 4 kPa in a 4 s period. However, as the model used in this work is idealised and lacks any geometrical changes, in practice unsafe pressure changes may be generated.

13
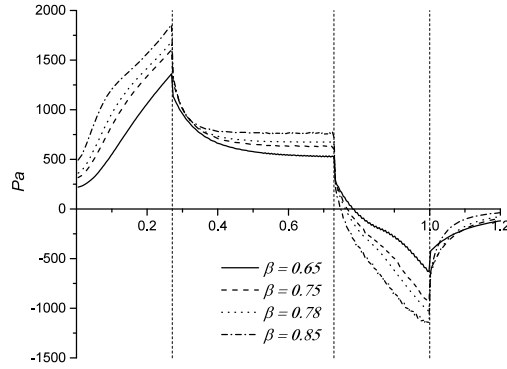
Figure 9: Pressure difference between train front and back.

### 7.1.3. Viscous and Pressure Drag

The drag coefficient can be considered as two separate components; the pressure ($C_D^P$) and the viscous ($C_D^V$) drag. Pressure drag arises due to the force of the air on the front facing surfaces while viscous drag arises from the friction between the air and the surfaces. The viscous and pressure drag coefficients are calculated using Equation (3) by replacing the total force with either the viscous or pressure force.

Figure 10 shows the total drag decomposed into its pressure and viscous components given as averages across the three phases of motion.
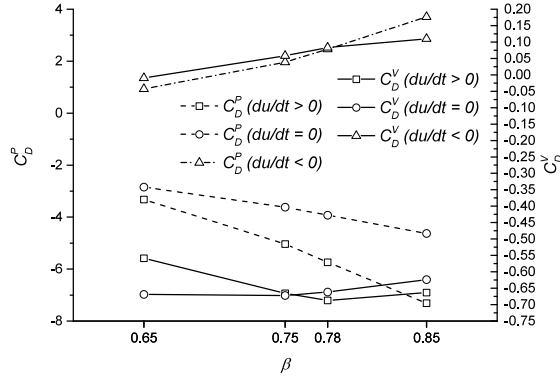


Figure 10: Pressure ($C_D^P$) and viscous ($C_D^V$) drag coefficients.

During the constant velocity phase the drag increases in magnitude with increasing blockage ratio, with the increase being dominated by an increase in pressure drag due to the large train cross section. There is also a contribution from friction pressure drag driven by the restriction in the annular region between train and tunnel. The viscous drag, while an important component in this phase, does not vary with blockage ratio significantly but contributes to pressure drag through the friction pressure drag. During deceleration the positive drag increases at a higher rate than the increase in magnitude during the constant velocity phase. During this phase the pressure drag is again most significant with the viscous drag having giving a small contribution. This is due to the low annular region flow relative to the train. During acceleration the pressure drag contribution increases with blockage ratio. The viscous drag contribution increases up to $\beta = 0.78$ after which only small changes are observed.

14

### 7.1.4. Displaced Air Volumes

Figure 11(a) shows the total tunnel outlet air flow and average drag coefficients for the three phases of train motion.
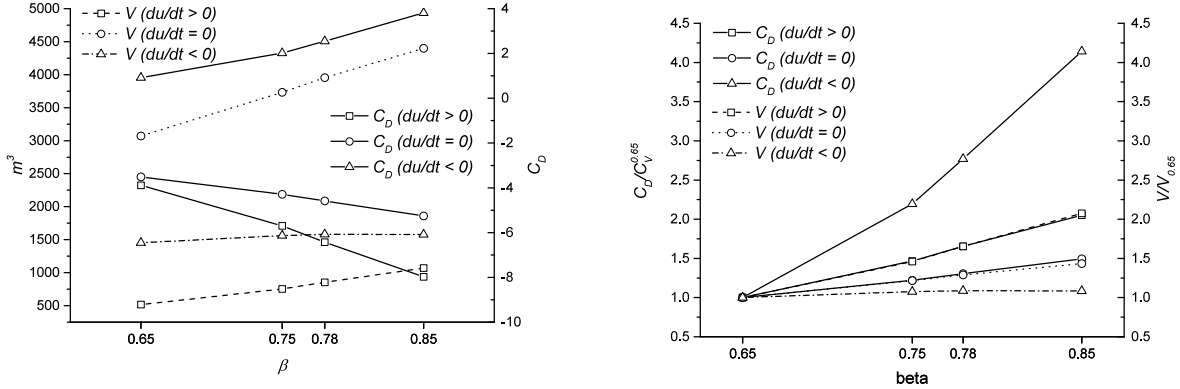


(a) Tunnel outlet air flow volume $(V)$ and average train drag coefficients $(C_D)$.

(b) Normalised coefficients, $(V/V^{0.65})$ and $(C_D/C_D^{0.65})$.

Figure 11: Tunnel outlet air flow volume and train drag coefficients during three phases of motion for various blockage ratios.

The increase in flow volume during acceleration and constant velocity phases are most significant. The air flow volume during deceleration shows a fairly insignificant increase. Negligible increases during deceleration are seen after $\beta = 0.75$. This is due to the restricted size of the annular region constricting the flow of air from the back to the front of the train. The results from Figure 11(a) are shown in Figure 11(b) normalised by the values of the respective quantity at $\beta = 0.65$.

This shows that the drag and outlet air flow volumes increase in an almost identical manner during acceleration and constant velocity phases but that the drag during deceleration increases very significantly (by a factor of 4) and that air flows show little change. Overall the air flow and drag increase by a factor of two during acceleration and by a factor of 1.4 during constant velocity.

Table 7 shows the total volume of air displaced from the tunnel outlet, also expressed as a fraction of the tunnel volume. As the blockage ratio is increased by 15%, from 0.65 to 0.75, the fraction of the tunnel volume displaced increases by 20%, from 0.52 to 0.63. A 30% increase in blockage ratio, from 0.65 to 0.85, increases by 40%, from 0.52 to 0.73. This implies a linear relationship between total displaced air and blockage ratio.

Table 7: Total displaced air for various $\beta$.

| $\beta$ | $V$ (m$^3$) | $V/V_t$ () |
|---|---|---|
| 0.65 | 5039.40 | 0.527 |
| 0.75 | 6047.71 | 0.633 |
| 0.78 | 6387.44 | 0.668 |
| 0.85 | 7046.84 | 0.737 |

### 7.2. Tunnel and Train Length Variation

The length of the train $(X_{tr})$ and tunnel $(X_t)$ in model $M_2$ with $Re_{max} = 8.215 \times 10^5$ are varied separately to examine the effect on the airflows. Model $M_2$ was chosen as this would allow comparison with a validated model and the specific $Re_{max}$ case was selected as a compromise between a higher velocity, for realism, and reducing computational time.

15

The train length was fixed at $60\,\text{m}$ and $X_t$ increased to $1170\,\text{m}$ and $1560\,\text{m}$. The tunnel length was then fixed at $1170\,\text{m}$ and the train length increased to $90\,\text{m}$, $120\,\text{m}$ and $150\,\text{m}$. These cases are referred to as $M_2(X_{tr}, X_t)$ with appropriate values of $X_{tr}$ and $X_t$

### 7.2.1. Effect on Drag and Velocity

The results obtained from variations in the tunnel and train lengths are presented at the end of the acceleration ($du/dt > 0$ case) and constant velocity ($du/dt = 0$ case) phases of the train motion, shown in Figure 12.



(a) Train length variation.

(b) Tunnel length variation.
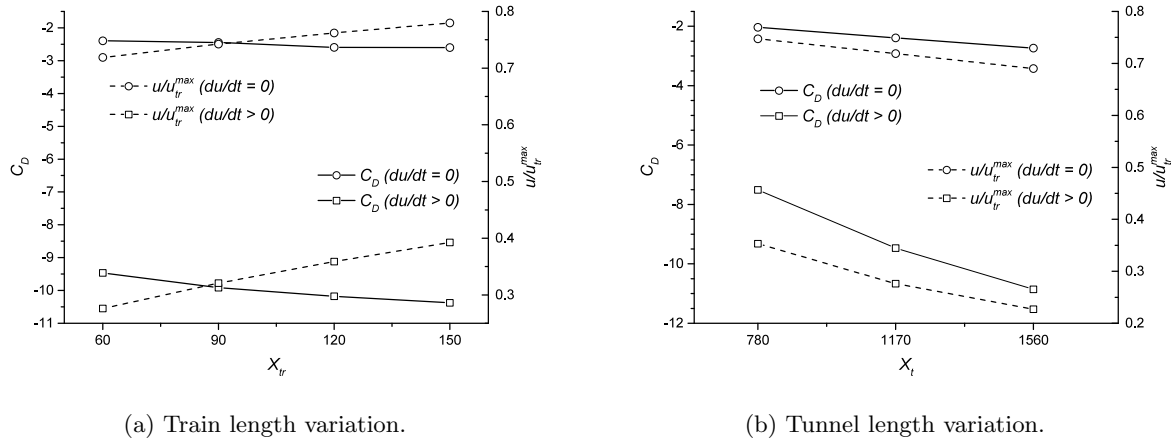
Figure 12: $C_D$ and $u/u_{tr}^{max}$ for train length variation for two phases of motion.

The patterns of the coefficients during the train motion are similar to those presented previously and so are omitted. In this section the trends during the acceleration and constant velocity phases are highlighted as representative of the flow.

Increasing train length increases the tunnel outlet velocity during both phases of motion. Doubling the train length results in a 33% increase in air velocity during acceleration and a 13% increase during constant velocity. During acceleration there is an increase in drag of around 10% while during constant velocity there is no significant increase.

Figure 12(b) shows the behaviour for variations of tunnel length. Doubling the tunnel length decreases the tunnel outlet velocity by around 33% during acceleration and increases the drag by 45%. During constant velocity the changes are less significant with a decrease of around 13% in outlet velocity and an increase of 50% in drag.

### 7.2.2. Viscous and Pressure Drag

Figures 13(a) and 13(b) show the decomposed drag coefficient for the various train and tunnel lengths during acceleration and constant velocity.

Figure 13(a) shows the decomposed drag for train length variation. It can clearly be seen that the pressure drag does not change significantly during either phase of motion. This is due to the train frontal area and annular region being constant and the volume of air opposing the train being largely similar. There are larger changes in the viscous drag which increase significantly due to the larger surface area of the train sides. As there is a longer annular region this creates more resistance to the air flow from train front to back, hence increasing the tunnel outlet velocity. The small increases in pressure drag are due to the increased viscous drag, a form of drag known as viscous pressure drag [25]. As the viscous drag does not contribute significantly to the drag the total drag does not increase significantly due to increasing train length.

Figure 13(b) shows the decomposed drag for tunnel length variation. The changes in pressure and viscous drag during constant velocity motion are not significant given that the change is total drag was also not

16

(a) Train length variation.          (b) Tunnel length variation.
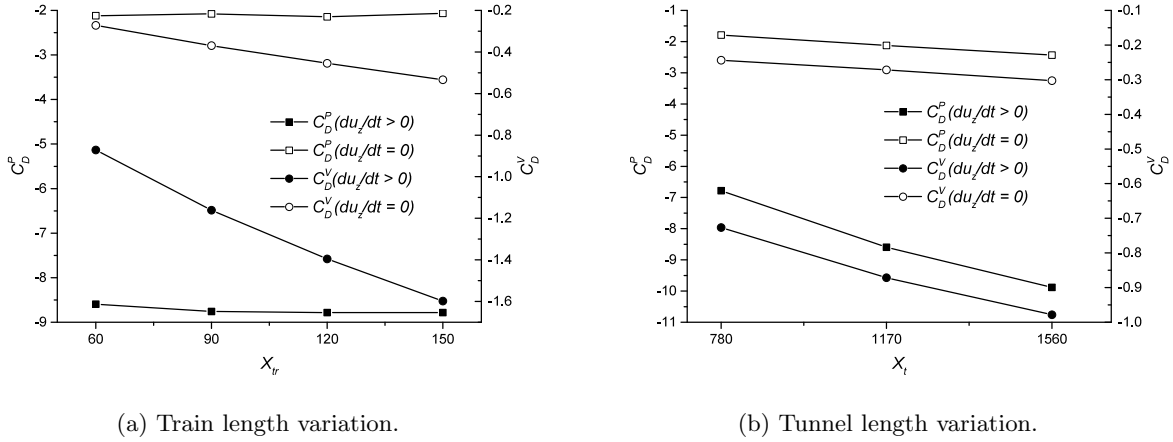
Figure 13: $C_D^P$ and $C_D^V$ for train and tunnel length variation.

significant. The pressure and viscous drag coefficients increase significantly during acceleration, although the viscous drag is not a large contributor to total drag.

### 7.2.3. Displaced Air Volumes

The total displaced air volumes for various train lengths are shown in Table 7. In this case the length of the tunnel is 1170 m.

Table 8: Total displaced air for various train lengths.

| $X_{tr}$ | $V$ (m$^3$) | $V/V_t$ () |
|----------|-------------|------------|
| 60       | 12314.36    | 0.501      |
| 90       | 12538.92    | 0.510      |
| 120      | 12538.84    | 0.510      |
| 150      | 12552.67    | 0.511      |

Generally the proportion of tunnel air displaced from the outlet is around 50% of the total tunnel volume. Increasing the train length by 250% from 60 m to 150 m results in an almost negligible increased in displaced air volume (around 2%).

The total displaced air volumes for various tunnel lengths are shown in Table 9. In this case the length of the train is 60 m.

Table 9: Total displaced air for various train lengths.

| $X_t$ | $V$ (m$^3$) | $V/V_t$ () |
|-------|-------------|------------|
| 780   | 8156.49     | 0.498      |
| 1170  | 12314.36    | 0.501      |
| 1560  | 16294.60    | 0.497      |

Again the proportion of tunnel air displaced from the outlet is around 50% of the total tunnel volume. Increasing the train length by 100% from 780 m to 1560 m results in an almost negligible increased in displaced air volume.

17

## 8. Conclusions

The transient, three-dimensional air flows in an underground railway have been modelled using computational fluid dynamics. A scale model was developed, based on published literature, and validated with available experimental data. The model was scaled geometrically and it was found that the flow behaviour was similar in both cases, thus demonstrating the validity of the numerical model. Reynolds number scaling was carried out to observe the behaviour of the air flows with similar trends found throughout the ranges tested.

The effect of increasing the blockage ratio was found to increase the air velocities at the tunnel outlet almost to the train maximum velocity for $\beta = 0.85$. It was found that drag increases by about 50% during constant velocity, 100% during acceleration and 300% during deceleration. Total air flow volumes displaced form the tunnel increase at broadly the same rate as drag for acceleration and constant velocity phases. During deceleration, the increase in displaced air volume plateaus at around $\beta = 0.75$. The effect of pressure drag was found to be more significant than viscous drag.

The train and tunnel lengths were varied and it was found that both strongly influenced the air flows in the tunnel. The train total drag was strongly influenced by tunnel length through increasing the pressure drag while the train length had a less significant impact only increasing the viscous drag. A longer train was found to increase tunnel outlet velocities by about 13% and generates no significant increases in drag during constant velocity. Overall no differences were found in the fraction of the tunnel volume displaced from the tunnel outlet.

The forces acting upon the train and the annular region air velocities have been highlighted. The behaviour during deceleration is shown as distinct from the other phases of travel; the body of air behind the train acts as a positive force upon it and air flows are restricted from moving from the tail to nose of the train. This will create a force against which the train brakes will need to work. The positive drag also indicates that the train blocks the movement of air flows ahead of it, minimising the potential for ventilating flows.

In this work it has been shown that the alteration of blockage ratio can increase ventilating air flows during train motion. While this has been shown further work is required to understand how this could be practically achieved in existing systems to enhance ventilation. Consideration of the trade off between higher blockage ratio and the heat generated because of a smaller annular gap is also required. A study of the highest blockage ratio which can practically be achieved physically is also necessary.

## 9. Acknowledgements

## References

[1] M. Botelle, P. McSheffrey, P. Zouzoulas, A. Burchell, Dubai metro: building the world's longest driverless metro, Proceedings of the ICE - Civil Engineering 165 (2012) 114–122.

[2] M. Botelle, K. Payne, B. Redhead, Squeezing the heat out of London's tube, Proceedings of the ICE - Civil Engineering 163 (2010) 114–122.

[3] Transit Development Corporation, Associated Engineers, Subway Environmental Design Handbook, National Technical Information Service, 1975.

[4] C. W. Pope, D. G. Newman, D. A. Henson, The factors affecting draught relief and air temperature in an underground metro system, in: Papers Presented at the 10th International Symposium on Aerodynamics and Ventilation of Vehicle Tunnels, volume 43, BHR Group, 2000, pp. 153–170.

[5] C.-J. Lin, Y. K. Chuah, C.-W. Liu, A study on underground tunnel ventilation for piston effects influenced by draught relief shaft in subway system, Applied Thermal Engineering 28 (2008) 372–379.

[6] D. C. Eckford, C. W. Pope, Cooling of Underground Railways, in: 12th International Symposium on Aerodynamics and Ventilation of Vehicle Tunnels, volume 1, BHR Group, Cranfield, UK, 2006, pp. 409–424.

[7] T. Ono, K. Iwai, K. Maeda, A new air conditioning and ventilation scheduling method for subway energy saving utilizing the wind driven by trains, in: 12th International Symposium on Aerodynamics and Ventilation of Vehicle Tunnels, volume 1, BHR Group, Cranfield, UK, 2006, pp. 437–450.

[8] J. Y. Kim, K. Y. Kim, Experimental and numerical analyses of train-induced unsteady tunnel flow in subway, Tunnelling and Underground Space Technology 22 (2006) 166–172.

[9] J.-Y. Kim, K.-Y. Kim, Effects of vent shaft location on the ventilation performance in a subway tunnel, Journal of Wind Engineering and Industrial Aerodynamics 97 (2009) 174–179.

[10] M.-T. Ke, T.-C. Cheng, W.-P. Wang, Numerical simulation for optimizing the design of subway environmental control system, Building and Environment 37 (2001) 1139–1152.

[11] E. M. El-Bialy, E. E. Khalil, Experimental and numerical investigation of indoor environmental quality in a subway station, in: Tenth International Congress of Fluid Dynamics, ICFD, 2010, pp. 1–6.

[12] W. Yan, G. Naiping, W. Lihui, W. Xiping, A numerical analysis of airflows caused by train-motion and performance evaluation of a subway ventilation system, Indoor and Built Environment (2013) 1–10.

[13] M. L. Gonzalez, M. G. Vega, J. M. F. Oro, E. B. Marigorta, Numerical modeling of the piston effect in longitudinal ventilation systems for subway tunnels, Tunnelling and Underground Space Technology 40 (2014) 22–37.

[14] P. Xue, S. You, J. Chao, T. Ye, Numerical investigation of unsteady airflow in subway influenced by piston effect based on dynamic mesh, Tunnelling and Underground Space Technology 40 (2014) 174–181.

[15] Y.-d. Huang, X.-l. Gong, Y.-j. Peng, C.-N. Kim, Effects of the solid curtains on natural ventilation performance in a subway tunnel, Tunnelling and Underground Space Technology 38 (2013) 526–533.

[16] F. Ampofo, G. Maidment, J. Missenden, Underground railway environment in the UK part 3: methods of delivering cooling, Applied Thermal Engineering 24 (2003) 647–659.

[17] P. Ricco, A. Baron, P. Molteni, Nature of pressure waves induced by a high-speed train travelling through a tunnel, Journal of Wind Engineering and Industrial Aerodynamics 95 (2007) 781 – 808.

[18] A. Baron, M. Mossi, S. Sibilla, The alleviation of the aerodynamic drag and wave effects of high-speed trains in very long tunnels, Journal of Wind Engineering and Industrial Aerodynamics 89 (2001) 365 – 401.

[19] Y.-Y. Ko, C.-H. Chen, I.-T. Hoe, S.-T. Wang, Field measurements of aerodynamic pressures in tunnels induced by high speed trains, Journal of Wind Engineering and Industrial Aerodynamics 100 (2012) 19 – 29.

[20] R. S. Raghunathan, H.-D. Kim, T. Setoguchi, Aerodynamics of high-speed railway train, Progress in Aerospace Sciences 38 (2002) 469 – 514.

[21] M. Howe, On the design of a tunnel-entrance hood with multiple windows, Journal of Sound and Vibration 273 (2004) 233 – 248.

[22] M. Bellenoue, B. Auvity, T. Kageyama, Blind hood effects on the compression wave generated by a train entering a tunnel, Experimental Thermal and Fluid Science 25 (2001) 397 – 407.

19

[23] J. Mok, J. Yoo, Numerical study on high speed train and tunnel hood interaction, Journal of Wind Engineering and Industrial Aerodynamics 89 (2001) 17 – 29.

[24] M. Rabani, A. K. Faghih, Numerical analysis of airflow around a passenger train entering the tunnel, Tunnelling and Underground Space Technology 45 (2015) 203 – 213.

[25] A. E. Vardy, Aerodynamic drag on trains in tunnels part 1: synthesis and definitions, Proceedings of the Institution of Mechanical Engineers, Part F: Journal of Rail and Rapid Transit 210 (1996) 29–38.

[26] A. E. Vardy, Aerodynamic drag on trains in tunnels part 2: prediction and validation, Proceedings of the Institution of Mechanical Engineers, Part F: Journal of Rail and Rapid Transit 210 (1996) 39–49.

[27] Y.-d. Huang, W. Gao, C.-N. Kim, A numerical study of the train-induced unsteady airflow in a subway tunnel with natural ventilation ducts using the dynamic layering method, Journal of Hydrodynamics, Ser. B 22 (2010) 164–172.

[28] Y.-d. Huang, X.-l. Gong, Y.-j. Peng, X.-y. Lin, C.-N. Kim, Effects of the ventilation duct arrangement and duct geometry on ventilation performance in a subway tunnel, Tunnelling and Underground Space Technology 26 (2011) 725–733.

[29] Ansys Inc., ANSYS ICEM CFD version 14.0, Canonsburg, PA, 2011. URL: `http://ansys.com`.

[30] Ansys Inc., ANSYS FLUENT version 14.0, Canonsburg, PA, 2011. URL: `http://ansys.com`.

[31] A. Khayrullina, B. Blocken, W. Janssen, J. Straathof, {CFD} simulation of train aerodynamics: Train-induced wind conditions at an underground railroad passenger platform, Journal of Wind Engineering and Industrial Aerodynamics 139 (2015) 100 – 110.

[32] S. Tavoularis, Measurement in fluid mechanics, Cambridge University Press, 2005.

[33] J. D. Anderson, Fundamentals of Aerodynamics, 4th ed., McGraw-Hill, 2007.

[34] A. Vardy, Unsteady airflows in rapid transit systems part 1: Measurements on the london transport victoria line, Proceedings of the Institution of Mechanical Engineers 194 (1980) 341–348.

[35] Transport for London, Rolling Stock Data Sheet, London, U.K., 2007. URL: `http://tfl.gov.uk`.

[36] F. E. Camelli, G. Byrne, R. Lhner, Modeling subway air flow using {CFD}, Tunnelling and Underground Space Technology 43 (2014) 20 – 31.

[37] International Union of Railways, Determination of railway tunnel cross-sectional areas on the basis of aerodynamic considerations, Paris, France, 2005. URL: `http://uic.org`.